CHEMISTRY OF MATERIALS
Cite This: Chem. Mater. XXXX, XXX, XXX−XXX
Article
pubs.acs.org/cm

Intercluster Reactions Resulting in Silver-Rich Trimetallic Nanoclusters

Esma Khatun, Papri Chakraborty, Betsy Rachel Jacob, Ganesan Paramasivam, Mohammad Bodiuzzaman, Wakeel Ahmed Dar, and Thalappil Pradeep*

Department of Chemistry, DST Unit of Nanoscience (DST UNS) and Thematic Unit of Excellence (TUE), Indian Institute of Technology Madras, Chennai 600036, India

Supporting Information

ABSTRACT: Herein, we present an intercluster reaction leading to new trimetallic nanoclusters (NCs) using bimetallic and monometallic NCs as reactants. Dithiol protected bimetallic $MAg_{28}(BDT)_{12}(PPh_3)_4$ (BDT = 1,3-benzenedithiol and M = Ni, Pd, or Pt) and monothiol protected $Au_{25}(PET)_{18}$ (PET = 2-phenylethanethiol) were used as model NCs. A mixture of trimetallic $MAu_xAg_{28-x}(BDT)_{12}(PPh_3)_4$ (x = 1−12) and bimetallic $Ag_xAu_{25-x}(PET)_{18}$ (x = 1−7) NCs were formed during the reaction as understood from time-dependent electrospray ionization mass spectrometry (ESI MS). Detailed studies of intercluster reaction between $Ag_{29}(BDT)_{12}(PPh_3)_4$ and $Au_{25}(PET)_{18}$ were also performed. Although both $MAg_{28}(BDT)_{12}(PPh_3)_4$ (M = Ag, Ni, Pd, or Pt) and $Au_{25}(PET)_{18}$ contain 13 atoms icosahedral core, only a maximum of 12 Au doped NCs were formed for the former as a major product and not the 13 Au doped one, unlike the previous reports of intercluster reaction. The transfer of Ni, Pd, or Pt atom from the center of icosahedron of $MAg_{28}(BDT)_{12}(PPh_3)_4$ to $Au_{25}(PET)_{18}$ was not observed, which suggests that the central atom is not involved in the reaction. Density functional theory (DFT) calculations were performed to know structures and properties of the formed NCs. This study demonstrates the use of intercluster reaction as an effective synthetic protocol to make multimetallic alloy NCs.

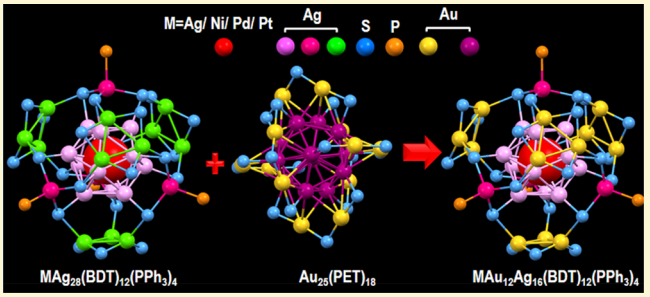

INTRODUCTION

Atomically precise nanoclusters (NCs) composed of an interior metal-core and exterior metal−ligand shell have gained significant attention due to their precise compositions and well-defined structures.[1−4] Robust stability of some NCs allows the growth of single crystals enabling structure determination by single-crystal X-ray diffraction leading to a detailed understanding of cluster-based materials.[5−8] They exhibit fascinating optical, catalytic, magnetic, and electrochemical properties which make them suitable for various applications.[9−14] The unique properties of NCs can be tuned by changing their structure, atomicity, protecting ligands, etc.[4,15−18] Among different NCs, alloy NCs composed of two or more metals are of great interest nowadays.[19−24] Alloying in Au and Ag NCs usually shows significant effects on catalysis, optics, etc., and therefore, it is of high importance in broadening their applications.[25−27] The very first example of an atomically precise bimetallic cluster synthesized was $PdAu_{24}(SR)_{18}$.[28,29] After that, many alloy NCs were synthesized which exhibited drastic change in structure and properties from their monometallic analogues. For example, 26-fold enhancement in photoluminescence (PL) was observed by the doping of 5 Au atoms in $Ag_{29}(BDT)_{12}(PPh_3)_4$ (BDT = 1,3-benzenedithiol and in short Ag_{29}).[30] Also, doping of Au increases the stability of NCs as observed in $Ag_{17}(TBBT)_{12}$ (*tert*-butylbenzenethiol).[31] Although poor stability of $Ag_{17}(TBBT)_{12}$ did not allow the formation of its single crystals, doping of one Au atom improved its stability and $AuAg_{16}(TBBT)_{12}$ was crystallized.[32] The effect of heteroatom doping in catalysis is well-studied.[12,33] Alloy NCs displayed higher catalytic activity than the monometallic analogues as observed in the oxidation of benzyl alcohol using Pd doped $Au_{25}(PET)_{18}$ (PET = 2-phenylethanethiol and in short Au_{25}).[34]

A wide variety of combinations and compositions are possible for alloy NCs.[35] Their structures depend on synthetic methods and conditions applied.[25] Among different synthetic procedures of alloy NCs, the most common procedures are coreduction, galvanic reduction, antigalvanic reduction, and intercluster reaction.[36−38] Depending on the metal atom and synthetic procedures, the doping position in alloy NCs can be defined which has significant effect on their properties.[22] A large number of alloy NCs have been synthesized by the coreduction method. However, it is hard to control the structures of the obtained alloy NCs. In the case of galvanic and antigalvanic reduction methods, structures and morphol-

Received: November 3, 2019
Revised: December 3, 2019
Published: December 4, 2019

DOI: 10.1021/acs.chemmater.9b04530
Chem. Mater. XXXX, XXX, XXX−XXX

ogy of the formed NCs depend on the metal precursor used in the reaction.[39] Properties of NCs depend on the morphology as in the case of sphere and rodlike Au_{25} NCs which showed different catalytic activity toward electro-reduction of CO_2.[40]

Intercluster reaction is a new and effective method for the synthesis of alloy NCs.[41] Krishnadas et al. introduced intercluster reactions between Au_{25} and $Ag_{44}(FTP)_{30}$ (FTP = 4-fluorothiophenol and in short Ag_{44}), which resulted in a mixture of bimetallic NCs.[42] Further, they studied the intercluster reaction between structurally similar Au and Ag NCs, Au_{25} and $Ag_{25}(DMBT)_{18}$ (DMBT = 2,4-dimethylbenzenethiol and in short Ag_{25}).[43] These intercluster reactions manifested the molecule-like reactions possible between atomically precise NCs. The bimetallic NCs formed during these reactions showed the conservation of structures. Other than these conventional methods, a new synthetic protocol was reported by Bürgi et al. where metal foils were used as doping reagents.[44] Their study revealed the importance of ligands and the metal-core during intercluster reactions. Though the reaction between monometallic NCs has been studied for the past several years, intercluster reaction using multimetallic NCs is still unexplored.

In this report, we have presented the formation of trimetallic NCs by intercluster reaction between dithiol protected bimetallic NCs, $MAg_{28}(BDT)_{12}(PPh_3)_4$ (M = Ni/Pd/Pt) (in short MAg_{28}) and a monothiol protected NC, Au_{25}. At first, we synthesized new bimetallic NCs, $PdAg_{28}$ and $NiAg_{28}$ along with the synthesis of known $PtAg_{28}$ by ligand exchange-induced structural transformation (LEIST) method starting from MAg_{24} NCs (M = Ni/Pd/Pt). The synthesized bimetallic NCs were used as precursors for the reaction with Au_{25} leading to the formation of trimetallic alloy NCs, $MAu_xAg_{28-x}(BDT)_{12}(PPh_3)_4$ (in short MAu_xAg_{28-x} where M is Ni/Pd/Pt and x = 1−12). Also, a detailed understanding of the intercluster reaction between Ag_{29} and Au_{25} has been presented which was not been addressed in our previous work.[45] The intercluster reaction between Ag_{29} and Au_{25} led to the formation of a mixture of bimetallic NCs, $Au_xAg_{29-x}(BDT)_{12}(PPh_3)_4$ (in short Au_xAg_{29-x} where x = 1−12) and $Ag_xAu_{25-x}(PET)_{18}$ (in short Ag_xAu_{25-x} where x = 1−7). Unlike the previous intercluster reactions where the metal-core was fully replaced by Au atoms, in this case, we found the formation of $Au_{12}Ag_{17}$ as the major product rather than $Au_{13}Ag_{16}$ upon completion of the reaction. The reaction between MAg_{28} and Au_{25} also resulted in the formation of $MAu_{12}Ag_{16}$ as the major product, which is understood as due to the reaction occurring at the surface of the NCs. The inner icosahedral core is seemingly protected by the metal-dithiol linkages in such a way that direct interaction with the metal-cores is not possible during the reaction. This was further confirmed from the fact that the central Ni, Pd, or Pt of MAg_{28} was not being transferred to Au_{25}. Further, theoretical calculations were carried out to understand structures and properties of the formed NCs.

RESULTS AND DISCUSSION

We synthesized bimetallic MAg_{24} (M = Ni/Pd/Pt) NCs following a reported protocol as mentioned in the Experimental Section. $NiAg_{24}$, synthesized for the first time, exhibited prominent absorption features at 483 and 665 nm (panel b in Figure S1A). The absorption maximum of $NiAg_{24}$ was 7 nm blue-shifted from that of Ag_{25} (panel a in Figure S1A). Panel b′ in Figure S1B presents ESI MS of $NiAg_{24}$ which exhibits a sharp peak at m/z 2558 with 2^- charge state corresponding to $[NiAg_{24}(DMBT)_{18}]^{2-}$. The formed $NiAg_{24}$ is stable at low temperature for a few months. However, at room temperature, it is less stable than Ag_{25}. Their absorption spectra at room temperature are presented in Figure S1C. Panels c/c′ and d/d′ in Figure S1 show UV−vis absorption spectra and ESI MS of $PdAg_{24}$ and $PtAg_{24}$, respectively, which are in accordance with the previous reports.[46]

The LEIST method was followed for the synthesis of unknown Ni/$PdAg_{28}$ and previously known $PtAg_{28}$ (details are given in the Experimental Section). Optical absorption spectrum of Ni-doped Ag_{29} shown in Figure 1A manifests a well-defined absorption peak at 440 nm along with a shoulder peak at 517 nm (green trace). The absorption maximum is 7 nm blue-shifted, while the shoulder peak is 4 nm red-shifted from that of Ag_{29} (red trace in Figure 1A).[47] An intense peak at m/z 1190 was observed along with a less intense peak at m/z 1587 in ESI MS which corresponded to $[NiAg_{28}(BDT)_{12}]^{4-}$ and $[NiAg_{28}(BDT)_{12}]^{3-}$, respectively (Figure 1B). Theoretical and experimental isotopic patterns of $[NiAg_{28}(BDT)_{12}]^{4-/3-}$ matched exactly with each other as shown in the inset of Figure 1B. The $NiAg_{28}$ got ionized at high pressure and high voltage conditions in which detachment of all PPh_3 ligands took place. On the other hand, the species did not get ionized at low voltage and low gas pressure conditions, and hence, we were unable to get PPh_3 attached peaks in ESI MS. X-ray photoelectron spectrum (XPS) of $NiAg_{28}$ given in Figure S2 shows the presence of Ag $3d_{5/2}$, Ni $2p_{3/2}$, P $2p_{3/2}$, and S $2p_{3/2}$ at 368.6, 853.9, 132.0, 163.0 eV, respectively. The $NiAg_{28}$ is more stable than the $NiAg_{24}$ which is revealed from their time-dependent absorption spectra presented in Figure S2B. It also shows good stability at high temperature (60 °C), although it is less stable than that of Ag_{29} as shown in Figure S2C.

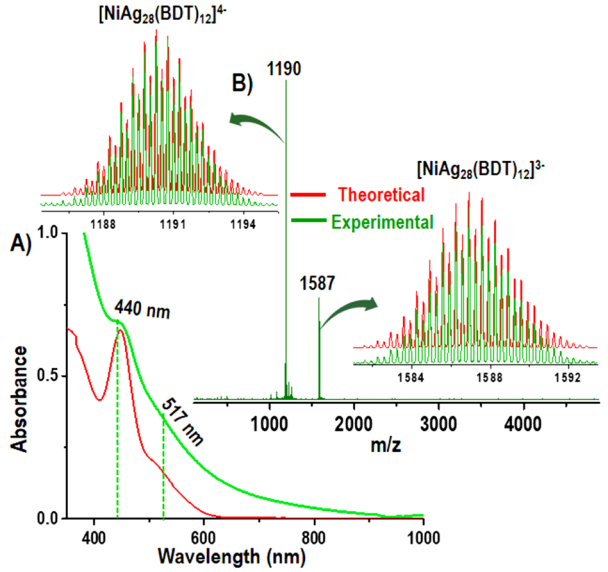

Figure 1. (A) UV−vis absorption spectrum of $NiAg_{28}$ (green trace), compared to Ag_{29} (red trace). (B) ESI MS of $NiAg_{28}$ which shows two peaks at m/z 1190 and 1587, corresponding to $[NiAg_{28}(BDT)_{12}]^{4-}$ and $[NiAg_{28}(BDT)_{12}]^{3-}$, respectively. Theoretical and experimental isotopic distributions of $[NiAg_{28}(BDT)_{12}]^{4-}$ and $[NiAg_{28}(BDT)_{12}]^{3-}$ are shown in the inset of (B) which match perfectly.

DOI: 10.1021/acs.chemmater.9b04530
Chem. Mater. XXXX, XXX, XXX−XXX

Pd doped Ag_{29} cluster was synthesized by the LEIST method which manifested distinct absorption features at 444 and 518 nm (Figure 2A). The absorption maximum (444 nm) was 3 nm blue-shifted than that of Ag_{29}, while the shoulder peak was ~5 nm red-shifted. ESI MS shown in Figure 2B consists of an intense peak at m/z 1202 along with a weak peak at m/z 1603. These correspond to 4^- and 3^- charge states of $[PdAg_{28}(BDT)_{12}]$. The presence of four PPh_3 ligands was confirmed by ESI MS measurement under low voltage and low gas pressure conditions (see Figure S3). $PdAg_{28}$ was also characterized with the help of other analytical tools such as XPS and secondary electron microscopy/energy dispersive X-ray spectroscopy (SEM/EDS) (Figure S4). XPS shows the presence of P, S, Pd, and Ag (Figure S4A). The Ag $3d_{5/2}$ peak appears at 368.5 eV which is at a higher value than that of Ag (0) (367.9 eV).

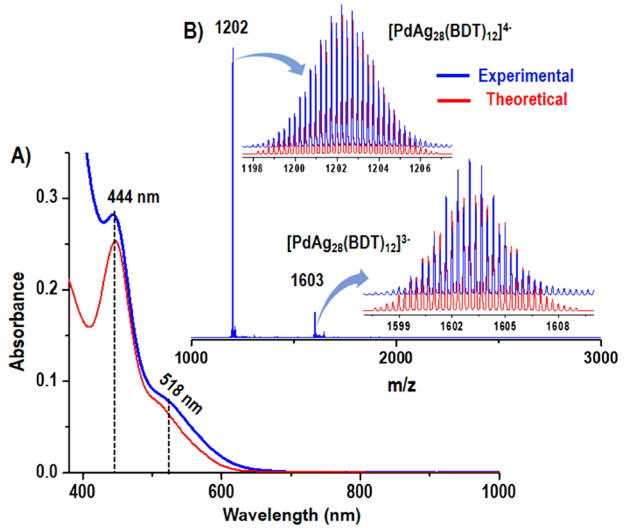

Figure 2. (A) UV−vis absorption spectrum of $PdAg_{28}$ having a maximum at ~444 nm (blue trace) is compared with that of Ag_{29} (red trace). (B) ESI MS of $PdAg_{28}$ which shows an intense peak at m/z 1202 corresponding to $[PdAg_{28}(BDT)_{12}]^{4-}$ along with a less intense peak at m/z 1603 corresponding to $[PdAg_{28}(BDT)_{12}]^{3-}$. Insets show experimental and theoretical isotopic distributions of $[PdAg_{28}(BDT)_{12}]^{4-}$ and $[PdAg_{28}(BDT)_{12}]^{3-}$ which fitted well with each other.

The Pd $3d_{5/2}$ peak appears at 337.5 eV which is also at a higher value than that of Pd (0) (335.5 eV). SEM/EDS characterization of the cluster is shown in Figure S4B. The elemental mapping clearly shows the presence of C, P, S, Ag, and Pd. The inset of Figure S4B shows the SEM image of the solid cluster and EDS mapping of the elements. Following a similar procedure, $PtAg_{28}$ was synthesized. Absorption spectrum presented in Figure S5A displays two prominent features at 425 and 491 nm which are in agreement with the previous report.[48] Two peaks at m/z 1224 and 1632 were noticed in ESI MS which are due to $[PtAg_{28}(BDT)_{12}]^{4-}$ and $[PtAg_{28}(BDT)_{12}]^{3-}$, respectively. Theoretical isotopic distribution of the peak at m/z 1224 matched exactly with the experimental one confirming the assignment of $[PtAg_{28}(BDT)_{12}]^{4-}$ (inset of Figure S5B). Unlike MAg_{24}, the MAg_{28} (M = Ni/Pd/Pt) clusters show both the 4^- and 3^- charge states which imply that Ni, Pd, or Pt act as both zerovalent and univalent dopants ($d^{10}s^0$ and d^9s^1), although the intensity of the zerovalent one is higher than the other.

For the sake of understanding the structure of the newly synthesized $NiAg_{28}$ and $PdAg_{28}$, we measured ESI MS as a function of collision energy (CE), and the data are presented in Figure S6. We observed the loss of smaller fragments such as $[Ag_5(BDT)_3]^-$ and $[Ag_3(BDT)_2]^-$ at higher CE. Ni or Pd atoms were not found in smaller fragments which suggest that Ni or Pd atoms do not occupy the staple motifs, rather they occupy the icosahedral core, similar to the case of $PtAg_{28}$.[48] This is because of their higher electronegativity similar to the previous reports.[26,46,49] Absorption spectra of both $NiAg_{28}$ and $PdAg_{28}$ are similar to Ag_{29}, suggesting that they have the same structures. Hence, we calculated the structures of $NiAg_{28}$ and $PdAg_{28}$ using density functional theory (DFT) and the most stable structures are presented in the insets of Figure 3A,B. Detailed descriptions of DFT calculations are given in the Experimental Section. Their optical absorption spectra calculated using time-dependent DFT (TDDFT) method are given in Figure 3A,B. They are consistent with the experimental ones, although there are some red-shifts (14 and 5 nm for $NiAg_{28}$ and $PdAg_{28}$, respectively) which are in accordance with the previous reports.[47,50] Other possible

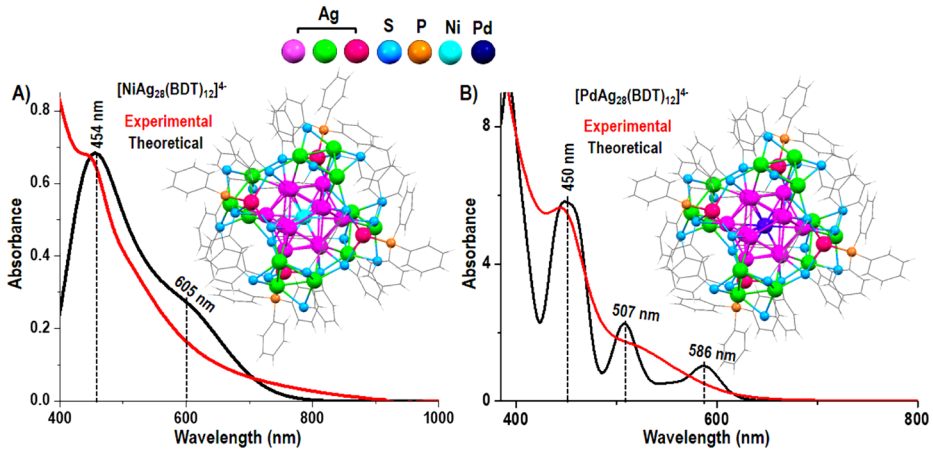

Figure 3. Theoretical (black) and experimental (red) UV−vis absorption spectra of (A) $NiAg_{28}$ and (B) $PdAg_{28}$. Insets of (A) and (B) show the DFT-calculated most stable structures of $NiAg_{28}$ and $PdAg_{28}$, respectively. Color code: light green, light pink, and pink denote Ag atoms, cyan denotes S atoms, orange denotes P atoms, sea blue denotes the Ni atom, and navy blue denotes the Pd atom.

DOI: 10.1021/acs.chemmater.9b04530
Chem. Mater. XXXX, XXX, XXX−XXX

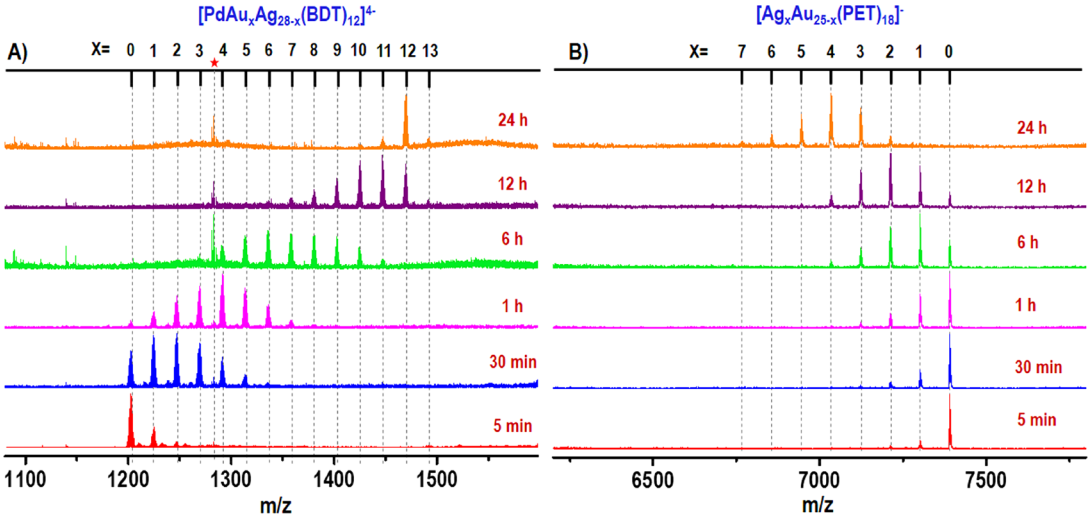

Figure 4. Time-dependent ESI MS of intercluster reaction between $PdAg_{28}$ and Au_{25} (1:5 ratio) where panel (A) shows the reaction at the $PdAg_{28}$ side and panel (B) presents the reaction at the Au_{25} side. The red asterisk corresponds to thiolates produced during the reaction. The species observed are $[PdAu_xAg_{28-x}(BDT)_{12}]^{4-}$ and $[Ag_xAu_{25-x}(PET)_{18}]^-$ abbreviated as $PdAu_xAg_{28-x}$ and Ag_xAu_{25-x}, respectively, and the charged species are not mentioned in the text for simplicity.

structures of $NiAg_{28}$ and $PdAg_{28}$ but higher in energy available from computations are shown in Figure S7.

Intercluster Reaction between $PdAg_{28}$ and Au_{25}. After the synthesis of bimetallic MAg_{28} (M = Ni/Pd/Pt) NCs and their thorough characterization, they were used for intercluster reaction with Au_{25}. At first, intercluster reactions between $PdAg_{28}$ and Au_{25} were performed for the synthesis of trimetallic $PdAu_xAg_{28-x}$ NCs (x = 1−12). From the time-dependent ESI MS of the reaction mixture of $PdAg_{28}$ and Au_{25} presented in Figure 4, it is evident that the intercluster reaction ended up with the formation of a stable trimetallic alloy NC, $PdAu_{12}Ag_{16}$ along with an unstable $PdAu_{13}Ag_{15}$ which disappeared with time. Along with the trimetallic NCs, bimetallic Ag_xAu_{25-x} (x = 1−7) NCs were also formed (Figure 4) as the final products. The rate of intercluster reaction between $PdAg_{28}$ and Au_{25} was found to be highly dependent on their molar ratio. To study the concentration dependence, we carried out reactions using different molar ratios of $PdAg_{28}$ and Au_{25} such as 4:1, 2:1, 1:1, 1:2, and 1:5, which are shown in Figure S8. The reaction rate was observed to be extremely slow when the amount of Au_{25} used was less than that of $PdAg_{28}$ (for 4:1 and 2:1 ratios of $PdAg_{28}$:Ag_{25}). Using a 1:1 ratio, we saw a satisfactory rate, although it took more than 1 day for the completion of the reaction. However, an increase in the amount of Au_{25} ($PdAg_{28}$:Ag_{25} = 1:5) led to the completion of the intercluster reaction within 24 h. Figure 4A shows that after 5 min, 2 Au atoms replace 2 Ag atoms to form $PdAu_xAg_{28-x}$ and consequently 2 Ag atoms replace 2 Au atoms, forming Ag_xAu_{25-x} where x is 0−2 (red traces in Figure 4A,B). But with increasing time, the number of doped Au atoms in $PdAg_{28}$ and doped Ag atoms in Au_{25} were not the same. After 30 min of reaction, we noticed that 6 Au atoms were doped in $PdAg_{28}$ while only 3 Ag atoms were doped in Au_{25} (blue traces in Figure 4A,B). At 1 h, 6 h, and 12 h, 8, 11, and 12 Au-doped $PdAg_{28}$, respectively, were formed while only 3, 4, and 5 Ag atom doping in Au_{25} were seen (pink, green, and violet traces, respectively, in Figure 4A,B). After 12 h, a small amount of 13 Au-doped product, $PdAu_{13}Ag_{15}$, was observed but when the reaction was continued up to 24 h, only 12 Au-doped product $PdAu_{12}Ag_{16}$ was formed as the main product (orange trace in Figure 4A). After 24 h, only up to 7 Ag-doped Au_{25} NCs were formed (orange trace in Figure 4B). Theoretical and experimental isotopic distributions of $PdAu_{12}Ag_{16}$ are presented in Figure S9 which fit well with each other, confirming the assigned composition. Time-dependent absorption spectra of the reaction mixture were measured, which are presented in Figure S10. The reaction mixture contains both trimetallic and bimetallic NCs as observed in ESI MS, but absorption spectra show the features of Ag_xAu_{25-x} (1−7). This is because of the higher Au_{25} concentration used in the reaction than $PdAg_{28}$ which masks the absorbance of $PdAg_{28}$. Interesting aspect in this intercluster reaction is that the Au atoms of Au_{25} are getting doped in $PdAg_{28}$ to make trimetallic NCs, while no Pd atom is getting inserted in Au_{25} to make the corresponding bi and trimetallic NC. To understand the mechanism, we studied other bimetallic NCs, $PtAg_{28}$ and $NiAg_{28}$ and performed their intercluster reactions with Au_{25}, and the data are discussed in the subsequent section.

Intercluster Reaction between $PtAg_{28}$ and Au_{25}. Time-dependent ESI MS of the intercluster reaction between $PtAg_{28}$ and Au_{25} ($PtAg_{28}$:Au_{25} = 1:5) is presented in Figure 5. Similar to $PdAg_{28}$, the intercluster reaction using $PtAg_{28}$ displayed systematic progress with time. The reaction was completed within 30 h which showed the formation of trimetallic $PtAu_{12}Ag_{16}$ NC as the major product (orange trace in Figure 5). Theoretical and experimental isotopic distributions of $PtAu_{12}Ag_{16}$ matched perfectly as shown in Figure S11. ESI MS of the reaction toward the Au_{25} side presented in Figure S12 manifests only 7 Au doping similar to the reaction between $PdAg_{28}$ and Au_{25}. Time-dependent absorption spectra are shown in Figure S13 which also reveal systematic change with time, and the final spectrum looks more like Ag_7Au_{18} NCs due to the use of higher concentration of Au_{25} than that of $PtAg_{28}$.

Intercluster Reaction between $NiAg_{28}$ and Au_{25}. To demonstrate the intercluster reaction between $NiAg_{28}$ and Au_{25}, we performed time-dependent ESI MS as shown in Figure S14. After 4 h of mixing, we found doping of 8 Au atoms in $NiAg_{28}$. Further monitoring of ESI MS was not possible due to the lower intensity of the formed trimetallic NCs. Therefore, we assume that similar to Pd and Pt, in the

DOI: 10.1021/acs.chemmater.9b04530
Chem. Mater. XXXX, XXX, XXX−XXX

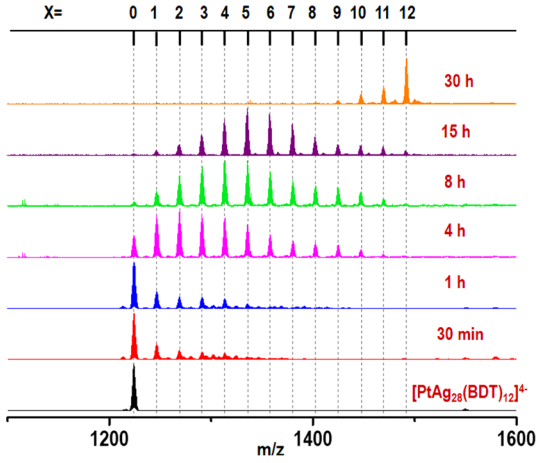

Figure 5. Time-dependent ESI MS of intercluster reaction between $PtAg_{28}$ and Au_{25} (1:5 ratio) showing the reaction at the $PtAg_{28}$ side. The reaction starts slowly and gets over within 30 h. The species formed are $[PtAu_xAg_{28-x}(BDT)_{12}]^{4-}$ abbreviated as $PtAu_xAg_{28-x}$, and the charged species are not mentioned in the text for simplicity.

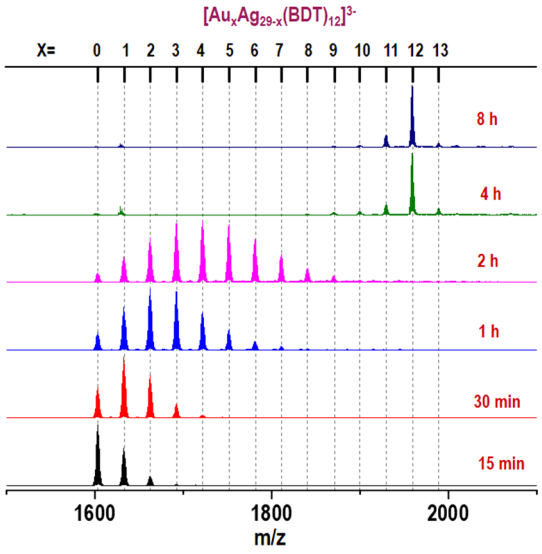

Figure 6. Time-dependent ESI MS of the reaction mixture of Ag_{29} and Au_{25} (Ag_{29}:Au_{25} = 1:5) at a higher temperature (60 °C). The reaction at the Ag_{29} side is shown here. The species observed are $[Au_xAg_{29-x}(BDT)_{12}]^{3-}$ abbreviated as Au_xAg_{29-x}, and the charged species are not mentioned in the text for simplicity.

case of $NiAg_{28}$, doping of 12 Au atoms is feasible, although we were unable to detect $NiAu_{12}Ag_{16}$ due to its lower ionization efficiency. Theoretical and experimental isotopic distributions of $NiAuAg_{27}$ are shown in Figure S15 which fit well with each other.

Intercluster Reaction between Ag_{29} and Au_{25}. To get more insight into the reaction mechanism, intercluster reaction between Ag_{29} and Au_{25} was performed in detail which was not mentioned in our previous report.[45] Similar to MAg_{28} (M = Ni/Pd/Pt), this reaction also required higher Au_{25} concentration in comparison to Ag_{29} (Figure S16). Time-dependent ESI MS corresponding to the reaction of 1:5 mixture of Ag_{29} and Au_{25} is presented in Figure S17. It exhibited a slower reaction rate than MAg_{28} (M = Ni/Pd/Pt) and was not completed even after 36 h. This is because of the lower reactivity of undoped NCs than the doped ones as evident from the previous reports.[51] To increase the rate, the reaction was carried out at a higher temperature which is shown in Figure 6. At 60 °C, the reaction was completed within 4 h which led to the formation of highly intense $Au_{12}Ag_{17}$ along with a small amount of $Au_{11}Ag_{18}$ and $Au_{13}Ag_{16}$ (see blue trace in Figure 6). Though Ag_{29} is having a similar Ag_{13} icosahedral core compared to Ag_{25}, $Au_{12}Ag_{17}$ was formed as a major product rather than $Au_{13}Ag_{16}$. The experimental isotopic distribution of $Au_{12}Ag_{17}$ is shown in Figure S18, which is in good agreement with the theoretical one. The reaction at Au_{25} side shows the insertion of 7 Ag atoms similar to the MAg_{28} (M = Ni/Pd/Pt), as shown in Figure S19. Time-dependent absorption spectra of the mixture shown in Figure S20 also display similar absorption features to that of the reaction product of MAg_{28} (M = Ni/Pd/Pt).

Mechanistic Details. Understanding the mechanism of a chemical reaction is an important aspect. According to the early reports of intercluster reactions, the metal−ligand interface plays an important role.[4,41] Hence, dithiol protected NCs exhibit slow reaction rate than the monothiol protected ones due to the stronger metal−ligand binding as well as higher intracluster noncovalent interactions between the protective ligands. In the case of monothiol protected NCs, the exchange of both metals and ligands were observed. However, for dithiol protected NCs, only metal exchange but no ligand exchange was feasible. It is also due to the strong binding of dithiol which cannot be replaced by a monothiol.[45]

In the previous example of intercluster reactions involving monothiol protected NCs such as Ag_{25} and Au_{25}, exchange of more than 12 atoms was observed during the reaction as they have more fluxional structures which were demonstrated by the Borromean ring model.[43] According to the Borromean ring model, NCs were viewed as a combination of three interlocked rings among which breakage of one ring can lead to the destruction of the whole structure during the reaction. Hence, the core atoms became easily accessible for interaction during the reaction which resulted in the doping of more than 12 atoms.[41,52] However, the structure of Ag_{29} (or MAg_{28}) is different from that of Ag_{25}. It has the Ag_{13} icosahedron protected by four Ag_3S_6 crown motifs and four $AgPPh_3$ units.[47] Out of the two kinds of staples present in Ag_{29}, crown-like Ag_3S_6 staples are easier to interact due to their less crowded surroundings as shown in Figure 7A. On the other hand, Au_{25} consists of Au_{13} icosahedron and six Au_2S_3 staples (shown in Figure 7A). During the reaction, there may be weak van der Waals interactions of one Ag_{29} with four Au_{25} approaching from four tetrahedral directions at different times in the process of reaction which may lead to the formation of $Au_{12}Ag_{17}$ at the end of the reaction. This kind of van der Waals interactions were feasible during the intercluster reaction between Ag_{25} and Au_{25}.[43] We suppose that 12 Au atoms occupy the crown motifs (see Figure 7B) of Ag_{29}. In an early report, 5 Au atoms were doped in Ag_{29} following the coreduction method. The crystal structure of $AuAg_{28}$ was reported where the Au atom occupies the central position. Further, the use of a higher amount of $AuPPh_3Cl$ led to the incorporation of more number of Au atoms which were incorporated at the terminal positions according to the NMR study. However, no crystal structure was reported for the higher number of Au doped NC.[30] In the case of intercluster reactions involving MAg_{28} (M = Ag/Ni/Pd/Pt) and Au_{25}, Ag atoms of the crown motifs get exchanged due to the geometry of approach of the two NCs during their interaction. Further,

DOI: 10.1021/acs.chemmater.9b04530
Chem. Mater. XXXX, XXX, XXX−XXX

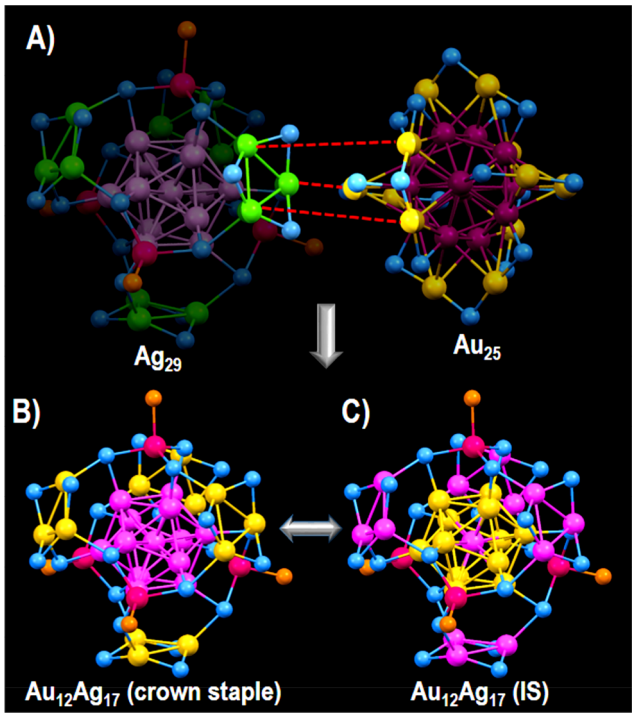

Figure 7. (A) The weak van der Waals interactions between staple metals of Ag_{29} and Au_{25} which results in (B) the formation of $Au_{12}Ag_{17}$ where Au atoms are doped in the crown motifs of Ag_{29}. (C) The rapid interchange between Au atoms on staples and Ag atoms on the icosahedral surface leads to the formation of a thermodynamically stable isomer of $Au_{12}Ag_{17}$.

the Au atoms present in crown motifs can rapidly interchange their positions to form other isomers which are energetically more stable.[53,54] There are four doping positions in MAg_{28} (M = Ag/Ni/Pd/Pt), among which the central atom is not getting replaced by Au atoms as we observed experimentally. Among the remaining three positions, icosahedral surface (IS) is energetically more stable (DFT calculated structure of $Au_{12}Ag_{17}$ is given in Figure 7C) than the other isomers as per DFT calculations. However, other isomers of $Au_{12}Ag_{17}$ also can exist in the solution, and their structures are shown in Figure S21. As $Ni/Pd/PtAg_{28}$ NCs are having similar structures to that of Ag_{29}, they exhibit the same reaction mechanism and form similar products. Also, $Ni/Pd/PtAu_{12}Ag_{16}$ possess similar structures to that of $Au_{12}Ag_{17}$ containing Ni, Pd, or Pt at the center of the icosahedron.

We used higher concentration of Au_{25} than Ag_{29} or MAg_{28} to speed up the reaction as discussed above which resulted in the doping of less number of Ag atoms in Au_{25} than the number of exchanges in Ag_{29} (experimentally, incorporation of 7 Ag atoms were observed). Similar to Ag_{29}, Ag atoms are supposed to dope first in the staple of Au_{25} during the reaction and then undergo rapid atom exchange to attain the energetically favored structure of Ag_xAu_{25-x} (x = 1−7) where Ag atoms are doped in the icosahedral surface positions.[55,56]

CONCLUSION

In conclusion, we discussed the formation of trimetallic NCs by intercluster reaction of bimetallic and monometallic NCs. We used dithiol protected MAg_{28} (M = Ni, Pd, or Pt) and monothiol protected Au_{25} for the reaction. The reaction was monitored by time-dependent ESI MS measurements. The reactions revealed that the central doped metal atoms, Ni, Pd, or Pt of MAg_{28} were unavailable for exchange by Au atoms and hence only Ag-rich trimetallic NCs got formed. At the end of the reaction, 12 Ag atoms of MAg_{28} were replaced by 12 Au atoms to form $MAu_{12}Ag_{16}$. The intercluster reaction between Ag_{29} and Au_{25} also showed the formation of $Au_{12}Ag_{17}$ as the major product. The study demonstrates that unlike the monothiol protected NCs, dithiol protected ones show strong metal−ligand binding due to the presence of strong non-covalent intracluster interactions between protective ligands. This led to the formation of $MAu_{12}Ag_{16}$ (M = Ag/Ni/Pd/Pt) by the outer metal−ligand shell interactions with Au_{25}. Therefore, inner cores were not involved in the reaction directly and remained unchanged. Intercluster reaction is thus found to be a useful tool to make multimetallic NCs that enrich the chemistry of atomically precise NCs.

EXPERIMENTAL SECTION

Materials and Chemicals. Sodium borohydride ($NaBH_4$, 95%), 1,3-benzenedithiol (BDT) (≥99%), 2,4-dimethylbenzenethiol (DMBT), 2-phenylethanethiol (PET), chloroauric acid trihydrate ($HAuCl_4{\cdot}3H_2O$), tetraoctylammonium bromide (TOAB), tetraphenylphosphonium bromide (PPh_4Br), palladium acetate ($Pd(OAc)_2$), nickel acetate ($Ni(OAc)_2$), chloroplatinic acid (K_2PtCl_4), and triethylamine were purchased from Sigma-Aldrich. Silver nitrate ($AgNO_3$) was purchased from Rankem chemicals. Triphenylphosphine (PPh_3, 98%) was purchased from Spectrochem. Dichloromethane (DCM), dimethylformamide (DMF), acetone, tetrahydrofuran (THF), and methanol (MeOH) were purchased from Rankem and were of HPLC grade. All chemicals were used without further purification.

Synthesis of $Au_{25}(PET)_{18}$ (Au_{25}). For the synthesis of Au_{25}, we followed a reported synthetic procedure.[57] About 40 mg of $HAuCl_4{\cdot}3H_2O$ was taken in 7.5 mL of THF and ∼65 mg of TOAB was added and stirred for 15 min to get a deep red solution. Next, ∼68 μL of PET was added, and the solution was stirred for 2 h to get a colorless solution indicating the formation of Au-SR. Then, the formed thiolate was reduced by adding ∼39 mg of $NaBH_4$ (in 2.5 mL of ice-cold water), and the stirring was continued for another 6−7 h to get a reddish-brown colored solution. After that, the reaction mixture was completely dried in rotavapor, and the cluster was precipitated by the addition of MeOH. The precipitate was washed thoroughly by MeOH to remove excess thiol and other impurities that were discarded with the supernatant solution. This washing was repeated for 2−3 times followed by the extraction of the Au_{25} cluster in acetone which helps to remove bigger particles and then the pure cluster was extracted in DCM.

Synthesis of $Ag_{25}(DMBT)_{18}$ (Ag_{25}). The cluster was synthesized following a reported method after a few modifications.[58] About 38 mg of $AgNO_3$ was dissolved in 5 mL of MeOH and then ∼9 mL of DCM was added to it. To this solution, ∼90 μL of DMBT was added which resulted in a thick yellow mixture. After 5 min, ∼6 mg of PPh_4Br (in 0.5 mL of MeOH) was added followed by the addition of 0.5 mL of an ice-cold aqueous solution of $NaBH_4$ (∼23 mg) after 20 min. The reaction mixture was stirred for ∼8 h and aged for 24 h. The dark brown solution was centrifuged, and then the supernatant was concentrated to ∼5 mL using a rotary evaporator. The cluster was precipitated by the addition of excess MeOH and washed several times with MeOH. Then the precipitate was dissolved in DCM and the cluster was extracted.

Synthesis of $MAg_{24}(DMBT)_{18}$ (MAg_{24} where M = Ni, Pd, or Pt). For the synthesis of $NiAg_{24}$, we followed a reported method after some modifications.[46] At first, ∼10 mg of $AgNO_3$ was dissolved in MeOH (5 mL) along with ∼10 mg of $Ni(OAc)_2$ (9 mL of DCM). Then, ∼10 μL of DMBT in 0.5 mL of DCM was added to the mixture followed by the addition of ∼10 mg of PPh_4Br (in 0.5 mL of DCM). After ∼20 min, $NaBH_4$ (40 mg in 0.5 mL of ice-cold water) was added, resulting in the reduction of Ag-Ni-phosphine-thiolate to form

DOI: 10.1021/acs.chemmater.9b04530
Chem. Mater. XXXX, XXX, XXX−XXX

NCs, and 50 μL of triethylamine was added after 5 min. The solution was kept stirring overnight. The formed cluster solution was evaporated and then washed with MeOH. The clusters were extracted in DCM. Following the similar synthetic route, $PtAg_{24}$ and $PdAg_{24}$ were synthesized using K_2PtCl_4 and $Pd(OAc)_2$, respectively, instead of $Ni(OAc)_2$.

Synthesis of $Ag_{29}(BDT)_{12}(PPh_3)_4$ (Ag_{29}). The cluster was synthesized adopting an already reported method.[47] First, ~20 mg of $AgNO_3$ was dissolved in 5 mL of MeOH, and then 9 mL of DCM was added. After a few mins, ~13.5 μL of BDT (0.5 mL of DCM) was added to the solution. Then, after 5 min of stirring in the dark, ~200 mg of PPh_3 (in 0.5 mL of DCM) was added to the mixture, and next, 0.5 mL of an ice-cold aqueous solution containing ~11 mg of $NaBH_4$ was added, which immediately changed the color of the solution to dark brown. The reaction was kept for 3 h under dark conditions. Then, the precipitate (red color) was collected by centrifugation and the concentrated solution was collected by rotary evaporation. The cluster was washed several times with MeOH and then dissolved in DCM. The reddish-orange colored cluster was collected after the removal of unwanted byproducts.

Synthesis of $MAg_{28}(BDT)_{12}(PPh_3)_4$ (MAg_{28} where M = Ni, Pd, or Pt). The ligand exchange induced structural/size transformation (LEIST)[8] method was used for the synthesis of MAg_{28}. MAg_{24} was taken in DCM as precursors, and then BDT and PPh_3 were added to the solution which was kept for 1 h. After that, DCM was evaporated and the formed cluster was washed with MeOH several times. Then, the cluster was extracted in DMF and used for further characterizations.

Synthesis of $MAu_xAg_{28-x}(BDT)_{12}(PPh_3)_4$ (MAu_xAg_{28-x} where M = Ni, Pd. or Pt; x = 1−13). The trimetallic clusters were prepared through the intercluster reaction between MAg_{28} and Au_{25}. MAg_{28} was taken in DMF and mixed with DCM solution of Au_{25}. Excess DMF was added to the mixture and then characterized using absorption spectroscopy and high-resolution electrospray ionization mass spectrometry (ESI MS).

Characterizations. Optical absorption spectra of samples were obtained using a PerkinElmer Lambda 25 spectrometer. Electrospray ionization (ESI) mass spectra (MS) of samples were measured using a Waters Synapt G2-Si high-resolution mass spectrometer. X-ray photoelectron spectra of samples were obtained using an Omicron ESCA Probe spectrometer with polychromatic Al Kα X-rays (hυ = 1486.7 eV). The pass energy for survey scans was kept at 50 eV during the measurements and changed to 20 eV for specific regions. Calibration of binding energies (BE) of the core levels was done with C 1s BE set at 285 eV. Secondary electron microscopic (SEM) measurements were done using FEI Quanta 200 operating at 30 kV equipped with energy-dispersive X-ray spectroscopy (EDS).

Computational Details. The structure and optical properties of $NiAg_{28}$, $PdAg_{28}$, and $Au_{12}Ag_{17}$ were calculated using density functional theory (DFT) and time-dependent DFT (TDDFT) which were implemented in Grid-Based Projector Augmented Wave method (GPAW).[59,60] In order to include only the interactions of the valence electrons, the PAW setup was considered as Ag($4d^{10}5s^{1}5p^{6}$), S($3s^{2}3p^{4}$), P($3s^{2}3p^{3}$), C($2s^{2}2p^{2}$), and H($1s^{1}$) with scalar relativistic effects which were included for Ag. Initially, the reported crystal structure of Ag_{29} was taken and the other structures were built up by replacing Ag atoms with Ni, Pd, and Au atoms. The geometry of all clusters was optimized using the PBE exchange function[61] in real-space finite difference (FD) mode in GPAW.51 having a grid spacing of 0.2 Å, and the convergence criterion for the forces on each atom was set to 0.05 eV/Å. Further, the optical absorption spectra were calculated by time-dependent DFT (TDDFT) using the optimized structures.[62]

■ ASSOCIATED CONTENT

Supporting Information

The Supporting Information is available free of charge at https://pubs.acs.org/doi/10.1021/acs.chemmater.9b04530.

UV−vis spectra, ESI MS, XPS, SEM/EDS, and theoretical analysis (PDF)

■ AUTHOR INFORMATION

Corresponding Author

E-mail: pradeep@iitm.ac.in.

ORCID

Thalappil Pradeep: 0000-0003-3174-534X

Notes

The authors declare no competing financial interest.

■ ACKNOWLEDGMENTS

We thank the Department of Science and Technology (DST) for supporting our research program. E.K. thanks IIT Madras for an institute doctoral fellowship. P.C. thanks the Council of Scientific and Industrial Research (CSIR) for a research fellowship. M.B. thanks U.G.C. for a research fellowship. G.P. thanks IITM for an Institute Postdoctoral Fellowship. W.A.D. thanks SERB-DST for the award of a National Postdoctoral fellowship. E.K. thanks Mr. Jyotirmoy Ghosh and Mr. M. P. Kannan for their help during XPS measurements.

■ REFERENCES

(1) Chakraborty, I.; Pradeep, T. Atomically Precise Clusters of Noble Metals: Emerging Link between Atoms and Nanoparticles. *Chem. Rev. (Washington, DC, U. S.)* **2017**, *117* (12), 8208−8271.

(2) Jin, R.; Zeng, C.; Zhou, M.; Chen, Y. Atomically Precise Colloidal Metal Nanoclusters and Nanoparticles: Fundamentals and Opportunities. *Chem. Rev. (Washington, DC, U. S.)* **2016**, *116* (18), 10346−10413.

(3) Xavier, P. L.; Chaudhari, K.; Baksi, A.; Pradeep, T. Protein-Protected Luminescent Noble Metal Quantum Clusters: An Emerging Trend in Atomic Cluster Nanoscience. *Nano Rev.* **2012**, *3* (1), 14767.

(4) Krishnadas, K. R.; Natarajan, G.; Baksi, A.; Ghosh, A.; Khatun, E.; Pradeep, T. Metal−Ligand Interface in the Chemical Reactions of Ligand-Protected Noble Metal Clusters. *Langmuir* **2019**, *35* (35), 11243−11254.

(5) Higaki, T.; Li, Q.; Zhou, M.; Zhao, S.; Li, Y.; Li, S.; Jin, R. Toward the Tailoring Chemistry of Metal Nanoclusters for Enhancing Functionalities. *Acc. Chem. Res.* **2018**, *51* (11), 2764−2773.

(6) Sakthivel, N. A.; Theivendran, S.; Ganeshraj, V.; Oliver, A. G.; Dass, A. Crystal Structure of Faradaurate-279: $Au_{279}(SPh\text{-}TBu)_{84}$ Plasmonic Nanocrystal Molecules. *J. Am. Chem. Soc.* **2017**, *139* (43), 15450−15459.

(7) Jensen, K. M. Ø.; Juhas, P.; Tofanelli, M. A.; Heinecke, C. L.; Vaughan, G.; Ackerson, C. J.; Billinge, S. J. L. Polymorphism in Magic-Sized $Au_{144}(SR)_{60}$ Clusters. *Nat. Commun.* **2016**, *7*, 11859.

(8) Zeng, C. Precision at the Nanoscale: On the Structure and Property Evolution of Gold Nanoclusters. *Pure Appl. Chem.* **2018**, *90* (9), 1409−1427.

(9) Tang, Q.; Hu, G.; Fung, V.; Jiang, D. E. Insights into Interfaces, Stability, Electronic Properties, and Catalytic Activities of Atomically Precise Metal Nanoclusters from First Principles. *Acc. Chem. Res.* **2018**, *51* (11), 2793−2802.

(10) Mathew, A.; Pradeep, T. Noble Metal Clusters: Applications in Energy, Environment, and Biology. *Part. Part. Syst. Charact.* **2014**, *31* (10), 1017−1053.

(11) Higaki, T.; Li, Y.; Zhao, S.; Li, Q.; Li, S.; Du, X.-S.; Yang, S.; Chai, J.; Jin, R. Atomically Tailored Gold Nanoclusters for Catalytic Application. *Angew. Chem., Int. Ed.* **2019**, *58* (25), 8291−8302.

(12) Tyo, E. C.; Vajda, S. Catalysis by Clusters with Precise Numbers of Atoms. *Nat. Nanotechnol.* **2015**, *10*, 577−588.

(13) Li, G.; Jin, R. Atomically Precise Gold Nanoclusters as New Model Catalysts. *Acc. Chem. Res.* **2013**, *46* (8), 1749−1758.

DOI: 10.1021/acs.chemmater.9b04530
Chem. Mater. XXXX, XXX, XXX−XXX

(14) Halawa, M. I.; Lai, J.; Xu, G. Gold Nanoclusters: Synthetic Strategies and Recent Advances in Fluorescent Sensing. *Mater. Today Nano* **2018**, *3*, 9−27.
(15) Joshi, C. P.; Bootharaju, M. S.; Bakr, O. M. Tuning Properties in Silver Clusters. *J. Phys. Chem. Lett.* **2015**, *6* (15), 3023−3035.
(16) Kang, X.; Zhu, M. Tailoring the Photoluminescence of Atomically Precise Nanoclusters. *Chem. Soc. Rev.* **2019**, *48* (8), 2422−2457.
(17) Li, G.; Abroshan, H.; Liu, C.; Zhuo, S.; Li, Z.; Xie, Y.; Kim, H. J.; Rosi, N. L.; Jin, R. Tailoring the Electronic and Catalytic Properties of Au_{25} Nanoclusters via Ligand Engineering. *ACS Nano* **2016**, *10* (8), 7998−8005.
(18) Du, Y.; Guan, Z.-J.; Wen, Z.-R.; Lin, Y.-M.; Wang, Q.-M Ligand-Controlled Doping Effects in Alloy Nanoclusters Au_4Ag_{23} and Au_5Ag_{24}. *Chem. - Eur. J.* **2018**, *24* (60), 16029−16035.
(19) Kumar, B.; Niihori, Y.; Kurashige, W.; Negishi, Y. Controlled Thiolate-Protected Gold and Alloy Clusters. In *Descriptive Inorganic Chemistry Researches of Metal Compounds*; InTech, 2017; p 13.
(20) Mohanty, J. S.; Xavier, P. L.; Chaudhari, K.; Bootharaju, M. S.; Goswami, N.; Pal, S. K.; Pradeep, T. Luminescent, Bimetallic AuAg Alloy Quantum Clusters in Protein Templates. *Nanoscale* **2012**, *4* (14), 4255−4262.
(21) Ferrando, R.; Jellinek, J.; Johnston, R. L. Nanoalloys: From Theory to Applications of Alloy Clusters and Nanoparticles. *Chem. Rev.* **2008**, *108* (3), 845−910.
(22) Jin, R.; Zhao, S.; Xing, Y.; Jin, R. All-Thiolate-Protected Silver and Silver-Rich Alloy Nanoclusters with Atomic Precision: Stable Sizes, Structural Characterization and Optical Properties. *CrystEngComm* **2016**, *18* (22), 3996−4005.
(23) Kang, X.; Abroshan, H.; Wang, S.; Zhu, M. Free Valence Electron Centralization Strategy for Preparing Ultrastable Nanoclusters and Their Catalytic Application. *Inorg. Chem.* **2019**, *58* (16), 11000−11009.
(24) Kang, X.; Wei, X.; Jin, S.; Yuan, Q.; Luan, X.; Pei, Y.; Wang, S.; Zhu, M.; Jin, R. Rational Construction of a Library of M_{29} Nanoclusters from Monometallic to Tetrametallic. *Proc. Natl. Acad. Sci. U. S. A.* **2019**, *116* (38), 18834−18840.
(25) Wang, S.; Li, Q.; Kang, X.; Zhu, M. Customizing the Structure, Composition, and Properties of Alloy Nanoclusters by Metal Exchange. *Acc. Chem. Res.* **2018**, *51* (11), 2784−2792.
(26) Liu, X.; Yuan, J.; Yao, C.; Chen, J.; Li, L.; Bao, X.; Yang, J.; Wu, Z. Crystal and Solution Photoluminescence of $MAg_{24}(SR)_{18}$ (M = Ag/Pd/Pt/Au) Nanoclusters and Some Implications for the Photoluminescence Mechanisms. *J. Phys. Chem. C* **2017**, *121* (25), 13848−13853.
(27) Yan, J.; Su, H.; Yang, H.; Hu, C.; Malola, S.; Lin, S.; Teo, B. K.; Häkkinen, H.; Zheng, N. Asymmetric Synthesis of Chiral Bimetallic $[Ag_{28}Cu_{12}(SR)_{24}]^{4-}$ Nanoclusters via Ion Pairing. *J. Am. Chem. Soc.* **2016**, *138* (39), 12751−12754.
(28) Fields-Zinna, C. A.; Crowe, M. C.; Dass, A.; Weaver, J. E. F.; Murray, R. W. Mass Spectrometry of Small Bimetal Monolayer-Protected Clusters. *Langmuir* **2009**, *25* (13), 7704−7710.
(29) Tofanelli, M. A.; Ni, T. W.; Phillips, B. D.; Ackerson, C. J. Crystal Structure of the $PdAu_{24}(SR)_{18}^{0}$ Superatom. *Inorg. Chem.* **2016**, *55* (3), 999−1001.
(30) Soldan, G.; Aljuhani, M. A.; Bootharaju, M. S.; AbdulHalim, L. G.; Parida, M. R.; Emwas, A.-H.; Mohammed, O. F.; Bakr, O. M. Gold Doping of Silver Nanoclusters: A 26-Fold Enhancement in the Luminescence Quantum Yield. *Angew. Chem., Int. Ed.* **2016**, *55* (19), 5749−5753.
(31) Wickramasinghe, S.; Atnagulov, A.; Yoon, B.; Barnett, R. N.; Griffith, W. P.; Landman, U.; Bigioni, T. P. $M_3Ag_{17}(SPh)_{12}$ Nanoparticles and Their Structure Prediction. *J. Am. Chem. Soc.* **2015**, *137* (36), 11550−11553.
(32) Conn, B. E.; Atnagulov, A.; Yoon, B.; Barnett, R. N.; Landman, U.; Bigioni, T. P. Confirmation of a de Novo Structure Prediction for an Atomically Precise Monolayer-Coated Silver Nanoparticle. *Sci. Adv.* **2016**, *2* (11), No. e1601609.
(33) Kwak, K.; Lee, D. Electrochemistry of Atomically Precise Metal Nanoclusters. *Acc. Chem. Res.* **2019**, *52* (1), 12−22.
(34) Xie, S.; Tsunoyama, H.; Kurashige, W.; Negishi, Y.; Tsukuda, T. Enhancement in Aerobic Alcohol Oxidation Catalysis of Au_{25} Clusters by Single Pd Atom Doping. *ACS Catal.* **2012**, *2* (7), 1519−1523.
(35) Hossain, S.; Niihori, Y.; Nair, L. V.; Kumar, B.; Kurashige, W.; Negishi, Y. Alloy Clusters: Precise Synthesis and Mixing Effects. *Acc. Chem. Res.* **2018**, *51* (12), 3114−3124.
(36) Ghosh, A.; Mohammed, O. F.; Bakr, O. M. Atomic-Level Doping of Metal Clusters. *Acc. Chem. Res.* **2018**, *51* (12), 3094−3103.
(37) Gan, Z.; Xia, N.; Wu, Z. Discovery, Mechanism, and Application of Antigalvanic Reaction. *Acc. Chem. Res.* **2018**, *51* (11), 2774−2783.
(38) Yang, S.; Chai, J.; Song, Y.; Fan, J.; Chen, T.; Wang, S.; Yu, H.; Li, X.; Zhu, M. In Situ Two-Phase Ligand Exchange: A New Method for the Synthesis of Alloy Nanoclusters with Precise Atomic Structures. *J. Am. Chem. Soc.* **2017**, *139* (16), 5668−5671.
(39) Wiley, B.; Sun, Y.; Chen, J.; Cang, H.; Li, Z.-Y.; Li, X.; Xia, Y. Shape-Controlled Synthesis of Silver and Gold Nanostructures. *MRS Bull.* **2005**, *30* (5), 356−361.
(40) Zhao, S.; Austin, N.; Li, M.; Song, Y.; House, S. D.; Bernhard, S.; Yang, J. C.; Mpourmpakis, G.; Jin, R. Influence of Atomic-Level Morphology on Catalysis: The Case of Sphere and Rod-Like Gold Nanoclusters for CO_2 Electroreduction. *ACS Catal.* **2018**, *8* (6), 4996−5001.
(41) Krishnadas, K. R.; Baksi, A.; Ghosh, A.; Natarajan, G.; Som, A.; Pradeep, T. Interparticle Reactions: An Emerging Direction in Nanomaterials Chemistry. *Acc. Chem. Res.* **2017**, *50* (8), 1988−1996.
(42) Krishnadas, K. R.; Ghosh, A.; Baksi, A.; Chakraborty, I.; Natarajan, G.; Pradeep, T. Intercluster Reactions between $Au_{25}(SR)_{18}$ and $Ag_{44}(SR)_{30}$. *J. Am. Chem. Soc.* **2016**, *138* (1), 140−148.
(43) Krishnadas, K. R.; Baksi, A.; Ghosh, A.; Natarajan, G.; Pradeep, T. Structure-Conserving Spontaneous Transformations between Nanoparticles. *Nat. Commun.* **2016**, *7* (1), 13447.
(44) Kazan, R.; Müller, U.; Bürgi, T. Doping of Thiolate Protected Gold Clusters through Reaction with Metal Surfaces. *Nanoscale* **2019**, *11* (6), 2938−2945.
(45) Ghosh, A.; Ghosh, D.; Khatun, E.; Chakraborty, P.; Pradeep, T. Unusual Reactivity of Dithiol Protected Clusters in Comparison to Monothiol Protected Clusters: Studies Using $Ag_{51}(BDT)_{19}(TPP)_3$ and $Ag_{29}(BDT)_{12}(TPP)_4$. *Nanoscale* **2017**, *9* (3), 1068−1077.
(46) Yan, J.; Su, H.; Yang, H.; Malola, S.; Lin, S.; Hakkinen, H.; Zheng, N. Total Structure and Electronic Structure Analysis of Doped Thiolated Silver $[MAg_{24}(SR)_{18}]^{2-}$ (M = Pd, Pt) Clusters. *J. Am. Chem. Soc.* **2015**, *137* (37), 11880−11883.
(47) AbdulHalim, L. G.; Bootharaju, M. S.; Tang, Q.; Del Gobbo, S.; AbdulHalim, R. G.; Eddaoudi, M.; Jiang, D.; Bakr, O. M. $Ag_{29}(BDT)_{12}(TPP)_4$: A Tetravalent Nanocluster. *J. Am. Chem. Soc.* **2015**, *137* (37), 11970−11975.
(48) Bootharaju, M. S.; Kozlov, S. M.; Cao, Z.; Shkurenko, A.; El-Zohry, A. M.; Mohammed, O. F.; Eddaoudi, M.; Bakr, O. M.; Cavallo, L.; Basset, J.-M. Tailoring the Crystal Structure of Nanoclusters Unveiled High Photoluminescence via Ion Pairing. *Chem. Mater.* **2018**, *30* (8), 2719−2725.
(49) Alkan, F.; Pandeya, P.; Aikens, C. M. Understanding the Effect of Doping on Energetics and Electronic Structure for Au_{25}, Ag_{25}, and Au_{38} Clusters. *J. Phys. Chem. C* **2019**, *123* (14), 9516−9527.
(50) Chen, T.; Yang, S.; Chai, J.; Song, Y.; Fan, J.; Rao, B.; Sheng, H.; Yu, H.; Zhu, M.; et al. Crystallization-Induced Emission Enhancement: A Novel Fluorescent Au-Ag Bimetallic Nanocluster with Precise Atomic Structure. *Sci. Adv.* **2017**, *3* (8), No. e1700956.
(51) Liu, Y.; Chai, X.; Cai, X.; Chen, M.; Jin, R.; Ding, W.; Zhu, Y. Central Doping of a Foreign Atom into the Silver Cluster for Catalytic Conversion of CO_2 toward C−C Bond Formation. *Angew. Chem., Int. Ed.* **2018**, *57* (31), 9775−9779.
(52) Natarajan, G.; Mathew, A.; Negishi, Y.; Whetten, R. L.; Pradeep, T. A Unified Framework for Understanding the Structure

DOI: 10.1021/acs.chemmater.9b04530
Chem. Mater. XXXX, XXX, XXX−XXX

and Modifications of Atomically Precise Monolayer Protected Gold Clusters. *J. Phys. Chem. C* **2015**, *119* (49), 27768−27785.
(53) Zheng, K.; Fung, V.; Yuan, X.; Jiang, D.-E.; Xie, J. Real-Time Monitoring of the Dynamic Intra-Cluster Diffusion of Single Gold Atoms into Silver Nanoclusters. *J. Am. Chem. Soc.* **2019**, *141*, 18977.
(54) Chakraborty, P.; Nag, A.; Natarajan, G.; Bandyopadhyay, N.; Paramasivam, G.; Panwar, M. K.; Chakrabarti, J.; Pradeep, T. Rapid Isotopic Exchange in Nanoparticles. *Sci. Adv.* **2019**, *5* (1), eaau7555.
(55) Kauffman, D. R.; Alfonso, D.; Matranga, C.; Qian, H.; Jin, R. A Quantum Alloy: The Ligand-Protected $Au_{25-X}Ag_x(SR)_{18}$ Cluster. *J. Phys. Chem. C* **2013**, *117* (15), 7914−7923.
(56) Kumara, C.; Aikens, C. M.; Dass, A. X-Ray Crystal Structure and Theoretical Analysis of $Au_{25-X}Ag_x(SCH_2CH_2Ph)_{18}^-$ Alloy. *J. Phys. Chem. Lett.* **2014**, *5* (3), 461−466.
(57) Bhat, S.; Baksi, A.; Mudedla, S. K.; Natarajan, G.; Subramanian, V.; Pradeep, T. $Au_{22}Ir_3(PET)_{18}$: An Unusual Alloy Cluster through Intercluster Reaction. *J. Phys. Chem. Lett.* **2017**, *8* (13), 2787−2793.
(58) Joshi, C. P.; Bootharaju, M. S.; Alhilaly, M. J.; Bakr, O. M. $[Ag_{25}(SR)_{18}]^-$: The "Golden"Silver Nanoparticle Silver Nanoparticle. *J. Am. Chem. Soc.* **2015**, *137* (36), 11578−11581.
(59) Enkovaara, J.; Rostgaard, C.; Mortensen, J. J.; Chen, J.; Dulak, M.; Ferrighi, L.; Gavnholt, J.; Glinsvad, C.; Haikola, V.; Hansen, H. A.; et al. Electronic Structure Calculations with GPAW: A Real-Space Implementation of the Projector Augmented-Wave Method. *J. Phys.: Condens. Matter* **2010**, *22* (25), 253202.
(60) Mortensen, J. J.; Hansen, L. B.; Jacobsen, K. W. Real-Space Grid Implementation of the Projector Augmented Wave Method. *Phys. Rev. B: Condens. Matter Mater. Phys.* **2005**, *71* (3), 035109.
(61) Perdew, J. P.; Burke, K.; Ernzerhof, M. Generalized Gradient Approximation Made Simple. *Phys. Rev. Lett.* **1996**, *77* (18), 3865−3868.
(62) Frisch, M. J.; Trucks, G. W.; Schlegel, H. B.; Scuseria, G. E.; Robb, M. A.; Cheeseman, J. R.; Scalmani, G.; Barone, V.; Mennucci, B.; Petersson, G. A.; et al. *Gaussian 09, revision B.01*; Gaussian, Inc.: Wallingford, CT, 2009.

DOI: 10.1021/acs.chemmater.9b04530
Chem. Mater. XXXX, XXX, XXX−XXX